Eur Biophys J (2011) 40:783–793
DOI 10.1007/s00249-011-0694-3

ORIGINAL PAPER

# Functional interactions between residues in the S1, S4, and S5 domains of Kv2.1

**E. Bocksteins · N. Ottschytsch · J.-P. Timmermans · A. J. Labro · D. J. Snyders**

Received: 3 August 2009 / Revised: 19 February 2011 / Accepted: 15 March 2011 / Published online: 1 April 2011


**Abstract** The voltage-gated potassium channel subunit Kv2.1 forms heterotetrameric channels with the silent subunit Kv6.4. Chimeric Kv2.1 channels containing a single transmembrane segment from Kv6.4 have been shown to be functional. However, a Kv2.1 chimera containing both S1 and S5 from Kv6.4 was not functional. Back mutation of individual residues in this chimera (to the Kv2.1 counterpart) identified four positions that were critical for functionality: A200V and A203T in S1, and T343M and P347S in S5. To test for possible interactions in Kv2.1, we used substitutions with charged residues and tryptophan for the outermost pair 203/347. Combinations of substitutions with opposite charges at both T203 and S347 were tolerated but resulted in channels with altered gating kinetics, as did the combination of negatively charged aspartate substitutions. Double mutant cycle analysis with these mutants indicated that both residues are energetically coupled. In contrast, replacing both residues with a positively charged lysine together (T203K + S347K) was not tolerated and resulted in a folding or trafficking deficiency. The nonfunctionality of the T203K + S347K mutation could be restored by introducing the R300E mutation in the S4 segment of the voltage sensor. These results indicate that these specific S1, S4, and S5 residues are in close proximity and interact with each other in the functional channel, but are also important determinants for Kv2.1 channel maturation. These data support the view of an anchoring interaction between S1 and S5, but indicate that this interaction surface is more extensive than previously proposed.

**Keywords** Voltage-gated $K^+$ channels · Charge mutations · Structure · Kv2.1 model

E. Bocksteins and N. Ottschytsch contributed equally to this work.

E. Bocksteins · N. Ottschytsch · A. J. Labro · D. J. Snyders (✉)
Laboratory for Molecular Biophysics,
Physiology and Pharmacology, Department of Biomedical Sciences, University of Antwerp, Universiteitsplein 1,
2610 Antwerp, Belgium
e-mail: dirk.snyders@ua.ac.be

J.-P. Timmermans
Laboratory of Cell Biology and Histology,
Department of Veterinary Sciences,
University of Antwerp, Antwerp, Belgium

## Introduction

Voltage-gated potassium (Kv) channels are transmembrane proteins consisting of four α-subunits that tetramerize to form a potassium-selective permeation pathway. Each subunit contains six transmembrane segments (S1–S6) with a pore loop (P) between S5 and S6 that contains the GYG signature sequence for potassium selectivity (Heginbotham et al. 1994). The N- and C-termini of each subunit are both located intracellularly. The segments S5-P-S6 are conserved from bacteria to mammalia and constitute the pore domain that forms the pathway for $K^+$ ions (Jiang et al. 2003; Long et al. 2005). The segments S1–S4 comprise the voltage-sensing domain (VSD) of the channel. These VSDs sense variations in membrane voltage and trigger a conformational change leading to the opening (or closing) of the central pore. The fourth transmembrane segment contains regularly spaced positive charges and is considered to be the main part of the voltage sensor (Bezanilla 2000). In 1998, the first crystal structure of a $K^+$ channel, KcsA, was obtained (Doyle et al. 1998). The bacterial KcsA channel is not a voltage-gated channel, and the α-subunits consist of only two transmembrane segments that are homologous to the S5-P-S6 domain of Kv channels. This structure has

been widely used as a model of the pore region of Kv channels and represents the closed conformation of the pore (Doyle et al. 1998). The question remains as to how the voltage-sensing S1–S4 segments are positioned against this pore region of a Kv channel. Mutagenesis, accessibility studies, cross-linking studies, etc. have been performed as an indirect approach to study the topology of the voltage-sensing parts and have been instrumental in developing hypothetical models of Kv channels (Durell et al. 2004; Gandhi and Isacoff 2002). Since 2005 at least two crystal structures of mammalian voltage-gated $K^+$ channels have been published: rat Kv1.2 (Long et al. 2005) and a Kv1.2 chimeric channel in which the voltage-sensor paddle of Kv1.2 was replaced with that from the Kv2.1 channel (Long et al. 2007).

In this study we investigate functional and structural relationships in the Kv2.1 channel for which a full crystal structure does not yet exist. In a previous study, chimeric channels were created in which domains of Kv2.1 were replaced with the corresponding domains of the silent subunit Kv6.4 (Ottschytsch et al. 2005). The latter does not form functional channels in homotetrameric configuration but does heterotetramerize with Kv2.1 subunits generating functional heterotetrameric Kv2.1/Kv6.4 channels (Ottschytsch et al. 2002). The Kv2.1 chimeras containing either the S1 or the S5 domain of Kv6.4 formed functional channels, although less efficiently (Ottschytsch et al. 2005), while a chimera that contained both the S1 and the S5 domain simultaneously was not able to generate current. Because substituting S1 or S5 of the nonfunctional Kv6.4 subunit individually in a Kv2.1 background was tolerated while replacing both segments simultaneously was not, we hypothesized that the S1 and S5 domains of the Kv2.1 channel interact with each other and thus would be in close proximity: if they interact, the substitution by one partner from Kv6.4 would be tolerated by the remaining WT partner, but not the double exchange. In the present study, we used a mutagenesis approach to gain more insight into the topology of S1 and S5 in the Kv2.1 channel structure. We show functional interactions between specific residues in the S1, S4, and the S5 segments of the Kv2.1 channel, which strongly suggests that these residues are in close proximity to each other.

## Methods

### Construction and mutagenesis of the S1–S5 chimera and Kv2.1

Human Kv2.1 and Kv6.4 [originally published as Kv6.3, but renamed by the IUPHAR gene nomenclature committee as Kv6.4 (Gutman et al. 2005; Ottschytsch et al. 2002)] were both cloned into the pEGFP-N1 vector (Clontech, Palo Alto, CA). The stop codon was removed by mutagenesis in such a way that the coding sequence of the channel was in frame with GFP, resulting in a C-terminally tagged subunit. Chimeric constructs were created using a loop-in PCR strategy (Ottschytsch et al. 2005). Site-directed mutagenesis was carried out using the QuikChange method (Stratagene, La Jolla, CA). All constructs obtained were verified by DNA sequencing.

### Cell culture and transfection

$Ltk^-$ cells were cultured at 37°C in DMEM supplemented with 10% horse serum and 1% penicillin/streptomycin under a 5% $CO_2$ atmosphere. For electrophysiological experiments, $Ltk^-$ cells were transiently transfected with 0.1–5 μg channel cDNA and 0.5 μg GFP using LipofectAMINE reagent according to the manufacturer's instructions (Invitrogen, San Diego, CA) and kept at 37°C or 25°C as indicated in the results. Twenty-four hours post-transfection the cells were trypsinized and used for analysis within 12 h.

### Confocal imaging

HEK293 cells were cultivated on coverslips in MEM supplemented with 10% fetal bovine serum and 1% penicillin/streptomycin and transfected with 0.5 μg GFP-tagged channel subunits using LipofectAMINE reagent (see above). After 48 h, confocal images were obtained on a Zeiss CLSM 510 equipped with an argon laser (excitation: 488 nm) for the visualization of GFP. Images were captured with a water immersion 40× C-apochromat (NA:1.2) objective, and the zoom factor was set between 5 and 7 in all scanning sessions. The thickness of the confocal slices was 1 μm. The images (resolution of 512 × 512 pixels) were further processed digitally using Zeiss LSM Image Browser and Corel Photo-paint.

### Whole-cell current recording

Current recordings were made with an Axopatch-200B amplifier (Axon instruments, Union City, CA) in the whole-cell configuration of the patch-clamp technique (Hamill et al. 1981). Experiments were performed at room temperature (20–23°C), and current recordings were low-pass filtered and sampled at 2–10 kHz with a Digidata 1200A data acquisition system (Axon Instruments). Command voltages and data storage were controlled with pClamp8 software (Axon Instruments). Patch pipettes were pulled with a laser puller (Sutter Instruments, Novato, CA) from 1.2 mm borosilicate glass (World Precision Instruments, Sarasota, FL). The cells were continuously perfused

with a bath solution containing (in mM) NaCl 145, KCl 4, $CaCl_2$ 1.8, $MgCl_2$ 1, HEPES 10, and glucose 10, adjusted to pH 7.35 with NaOH. The pipettes were filled with intracellular solution containing (in mM) KCl 110, $K_4$BAPTA 5, $K_2$ATP 5, $MgCl_2$ 2, and HEPES 10, adjusted to pH 7.2 using KOH. Junction potentials were zeroed with the filled pipette in the bath solution. The patch pipettes had resistances <3 MΩ. After achieving a gigaohm seal, the whole cell configuration was achieved by suction. The access resistance ranged from 3 to 9 MΩ. After compensation the series resistance was kept below 3 MΩ to ensure that voltage errors were <5 mV. Data from experiments in which the voltage error exceeded 5 mV were discarded.

### Data analysis

The voltage-dependence of channel activation and inactivation was fitted with a Boltzmann equation: $y = 1/(1 + \exp[-(E - V_{1/2})/k])$, in which k represents the slope factor, E the applied voltage, and $V_{1/2}$ the voltage at which 50% of the channels are activated or inactivated respectively. Both $V_{1/2}$ and the slope factor k were used to calculate the Gibbs free energy of activation at 0 mV ($\Delta G_0$): $\Delta G_0 = 0.0002389 z F V_{1/2}$, with the factor 0.0002389 to express the values in kcal/mol. $\Delta\Delta G_0$ was calculated as $[(\Delta G_0^{WT} - \Delta G_0^{mutant1}) - (\Delta G_0^{mutant2} - \Delta G_0^{mutant1+2})]$ with standard errors calculated using linear error propagation (Yifrach and MacKinnon 2002). To quantify the significance of coupling between residues, a cutoff value of 1 kcal/mol was chosen for the $\Delta\Delta G_0$ calculations. Time constants of activation and deactivation were obtained by fitting the current recordings to a mono-exponential function.

### Modeling of Kv2.1

Starting from the latest X-ray structure of Kv1.2 from rat (PDB code: 2R9R) (Long et al. 2007), hKv2.1 was homology modelled using the automated protein modelling server Swiss-Model (http://swissmodel.expasy.org//SWISS-MODEL.html) (Guex and Peitsch 1997). Sequence alignment of hKv2.1 with rKv1.2 was generated using ClustalX with minimal manual adjustment. After energy minimalization, the generated hKv2.1 homology model was analyzed with protein model check of the molecular modelling package WhatIf (http://swift.cmbi.kun.nl/WIWWWI/) (Vriend 1990). The pdb file of the hKv2.1 homology model is available upon request.

## Results

Previous results showed that replacing the S1 or the S5 transmembrane domain in Kv2.1 individually with the corresponding domains of the silent subunit Kv6.4 was tolerated (Ottschytsch et al. 2005). The resulting chimeric channels (S1 chimera and S5 chimera) generated delayed rectifier currents upon depolarization (Fig. 1). However, when both the S1 and S5 segments of Kv2.1 were replaced simultaneously with their Kv6.4 counterparts, the resulting chimera (S1/S5 chimera) was not functional, since no currents could be evoked upon depolarization between −100 and +70 mV (Fig. 1).

Alignment of the S1 and S5 segments showed strong sequence conservation between Kv2.1 and Kv6.4 in the S5 segment (60% identity) but much less so in the S1 segment (30% identity) (Fig. 2a). To investigate whether specific residues in the S1 and S5 segments of the chimera caused this loss of function, a mutagenesis approach was used. In the S1/S5 chimera, the S1 or S5 residues that differed between Kv6.4 (black residues) and Kv2.1 (red residues) were mutated back to Kv2.1 residues. Each mutation was tested for the ability to produce voltage-gated $K^+$ currents upon depolarization (Fig. 2b). Four positions were identified where a back mutation was able to restore the functionality of the S1/S5 chimera: A200V (yielding a current

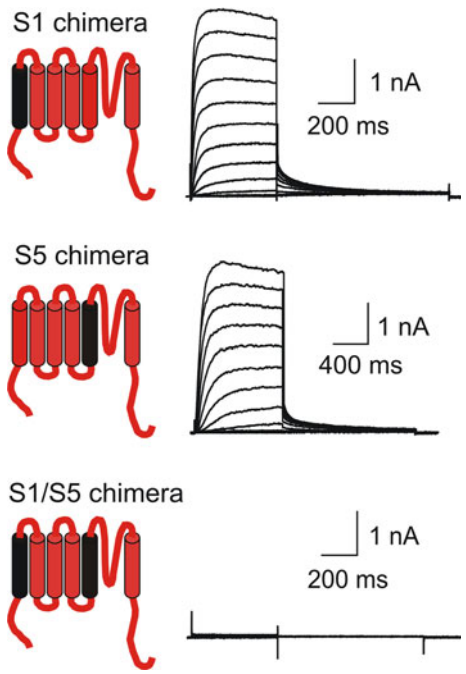


**Fig. 1** Schematic representation and whole cell current recordings of the S1 chimera, S5 chimera, and S1/S5 chimera. The cartoons show Kv2.1 domains colored *red*, while Kv6.4 domains are colored *black*. *On the right of each cartoon*, typical recordings from cells expressing the chimeric subunits are shown. The holding potential was −80 mV, and cells were depolarized in 10 mV increments from −60 mV to +70 mV, 500 ms in duration, followed by a repolarizing step at −25 mV, 850 ms in duration. For the S5 chimera with slower kinetics, the durations were doubled. The S1 chimera and the S5 chimera were functional, while the chimera that contains both transmembrane segments, the S1/S5 chimera, was not

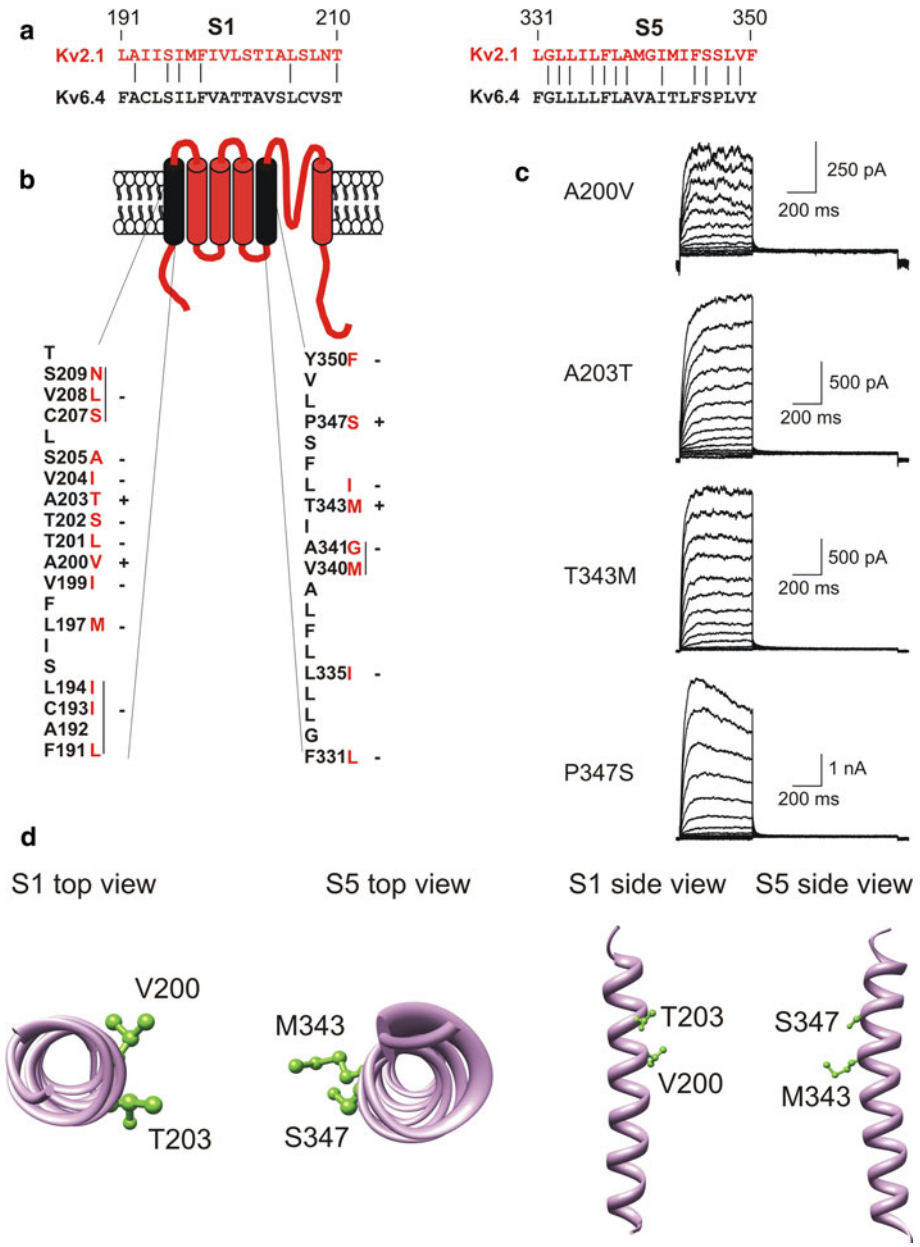


**Fig. 2a–d** Rescue mutations in the S1/S5 chimera. **a** Sequence alignments of the S1 and S5 segments of Kv2.1 (*red residues*) and Kv6.4 (*black residues*). Identical residues are indicated by a *connecting line*. **b** Cartoon of the S1/S5 chimera and the applied mutations. Kv2.1 and Kv6.4 sequences are colored *red* and *black*, respectively. Each Kv6.4 residue in S1 and S5 that differed from those of Kv2.1 was substituted by the Kv2.1 sequence. Simultaneous mutation of multiple residues is indicated by a *vertical line*. Each mutation was analyzed for expression of voltage-gated $K^+$ currents. A channel that displayed current is indicated by '+', a channel that never displayed current is indicated by '−'. **c** Typical current traces of the A200V, A203T, T343M, and P347S mutations in the S1/S5 chimera background. The holding potential was −80 mV, and cells were depolarized in 10 mV increments from −60 mV to +70 mV, 500 ms in duration, followed by a pulse at −35 mV, 850 ms in duration. **d** Top and side views of the S1 and S5 segments of our Kv2.1 homology model (see also Fig. 5a, b below). The four residues that rescued the S1/S5 chimera (V200, T203 in S1 and M343, S347 in S5) are shown in *green*. V200 and T203 are located on the same side of the S1 helix. M343 and S347 are located on the same side of the S5 helix

density of 120 ± 20 pA/pF at +70 mV, $n = 16$) and A203T (500 ± 110 pA/pF, $n = 12$) in S1 and T343M (400 ± 90 pA/pF, $n = 13$) and P347S (270 ± 80 pA/pF, $n = 15$) in S5 (Fig. 2c). These values were all substantially lower than the expression of WT Kv2.1 under similar conditions (Table 1). None of the other mutations produced any detectable currents (data not shown). The four residues were mapped on the α-helical S1 and S5 segments of our Kv2.1 homology model (Fig. 2d; see also Fig. 5 below). In this case V200 and T203 are located one turn apart on the

**Table 1** Electrophysiological properties of Kv2.1 and the functional mutations

| | Voltage dependence | | | | | | ΔΔG (kcal/mol) | Time constants (ms) | | | | Current density (pA/pF) | |
|---|---|---|---|---|---|---|---|---|---|---|---|---|---|
| | Activation | | | Inactivation | | | | Activation | | Inactivation | | | |
| | V½ (mV) | *k* | *n* | V½ (mV) | *k* | *n* | | At V½ +30 mV | *n* | At V½ −70 mV | *n* | At 70 mV | *n* |
| Kv2.1 | 12 ± 1 | 9 ± 1 | 11 | −16 ± 1 | 7 ± 1 | 5 | | 56 ± 5 | 7 | 15 ± 1 | 7 | 970 ± 180 | 15 |
| T203K | 17 ± 1 | 10 ± 1 | 7 | −13 ± 1 | 6 ± 1 | 6 | | 28 ± 4* | 7 | 8 ± 1 | 5 | 350 ± 110 | 17 |
| T203D | 13 ± 1 | 11 ± 1 | 9 | −22 ± 1 | 7 ± 1 | 7 | | 50 ± 4 | 7 | 17 ± 3 | 5 | 390 ± 90 | 20 |
| S347K | 18 ± 1 | 12 ± 1 | 6 | −24 ± 1 | 7 ± 1 | 7 | | 28 ± 4* | 7 | 13 ± 2 | 5 | 80 ± 20* | 9 |
| S347D | −16 ± 1* | 10 ± 1 | 6 | −43 ± 2* | 5 ± 1 | 6 | | 63 ± 9 | 5 | 34 ± 11 | 5 | 440 ± 140 | 11 |
| T203K + S347D | 6 ± 1 | 14 ± 1 | 8 | −35 ± 1* | 7 ± 1 | 6 | 0.98 ± 0.20 | 92 ± 10* | 7 | 37 ± 4* | 7 | 20 ± 10* | 9 |
| T203D + S347K | 28 ± 4* | 13 ± 1 | 6 | −42 ± 2* | 11 ± 1 | 6 | 0.47 ± 0.26 | 91 ± 6* | 6 | 11 ± 1 | 6 | 320 ± 70 | 11 |
| T203K + S347K | – | – | | – | – | | | – | | – | | | |
| T203D + S347D | 9 ± 1 | 16 ± 1 | 6 | −40 ± 1* | 9 ± 1 | 6 | 1.36 ± 0.18 | 96 ± 6* | 5 | 38 ± 1* | 6 | 50 ± 20* | 10 |
| T203W | 26 ± 7 | 18 ± 2 | 4 | −37 ± 2* | 7 ± 1 | 3 | | 22 ± 4* | 4 | 18 ± 1 | 2 | 230 ± 50* | 21 |
| S347W | −1 ± 2* | 12 ± 1 | 6 | −29 ± 1* | 5 ± 1 | 4 | | 53 ± 5* | 3 | 77 ± 9* | 3 | 320 ± 130 | 11 |
| T203W + S347W | 25 ± 2* | 18 ± 2 | 6 | −39 ± 2* | 10 ± 1 | 5 | 0.80 ± 0.30 | 90 ± 7* | 5 | 36 ± 6 | 5 | 280 ± 90* | 12 |
| T203K + S347K + R300E | 24 ± 2* | 12 ± 1 | 6 | −12 ± 1 | 8 ± 1 | 4 | | 27 ± 3* | 6 | 9 ± 2 | 6 | 11 ± 2* | 19 |

Values are given as mean ± S.E.M. with *n* the number of cells analyzed. Current densities were determined by transfecting 100 ng DNA. For the statistical analysis all values were compared to WT Kv2.1. *$p < 0.01$

same side of the S1 helix, which is also the case for M343 and S347 on the S5 helix.

A possible explanation for these results would be a direct interaction between residues in S1 and S5 pointing towards each other. We investigated this for the upper residue pair, T203 in S1 and S347 in S5, of the wild type Kv2.1 channel. We decided to perform all further experiments in the wild type Kv2.1 channel because of the possibility that the chimeric channel does not represent the correct conformation of Kv2.1. First both residues were mutated to cysteine to perform cross linking experiments, but the attempted experiments with the double cysteine mutant T207C + S347C using 2 mM DTT or 1 μM $Cd^{2+}$ were inconclusive as no changes in current amplitude or gating kinetics were observed (data not shown).

Next both residues were mutated to charged residues based on the hypothesis that if T203 and S347 of the Kv2.1 channel come in close contact, then similar charges might cause sufficient electrostatic repulsion to result in altered gating properties (or even nonfunctional channels), while opposite charges might be tolerated. As a control the single mutations were investigated first. These single charge mutations T203K, T203D, S347K, and S347D were all functional, generating outward currents comparable to Kv2.1 (Fig. 3a), with faster activation kinetics for the lysine substitutions (Table 1). In addition, the S347D mutation had a significant impact on channel gating, as this mutation shifted the voltage dependence of activation by approximately 28 mV in the hyperpolarized direction (Table 1). The double mutations with opposite charges (T203K + S347D and T203D + S347K) were both functional (Fig. 3b) but also affected channel gating (Table 1). Next we performed double mutant cycle analysis to test whether the mutations affect channel gating in a coupled way or independently. In the latter case, the resulting calculated $\Delta\Delta G_0$ value is close to zero. Calculating $\Delta\Delta G_0$ yielded a value of 0.98 ± 0.20 kcal/mol ($n = 9$) and 0.47 ± 0.26 kcal/mol ($n = 11$) for the double mutants T203K + S347D and T203D + S347K, respectively. For mutations with the same charge in S1 and S5, the double aspartate mutation (T203D + S347D) displayed voltage-gated $K^+$ currents, albeit with reduced amplitudes (Fig. 3b) and altered biophysical properties (Table 1). Double mutant cycle analyses yielded a $\Delta\Delta G_0$ value of 1.36 ± 0.18 kcal/mol for the double mutant T207D + S347D ($n = 10$), indicating that both residues are energetically coupled. In contrast, the double lysine substitution (T203K + S347K) was not tolerated (Fig. 3b). To investigate whether this lack of current was due to folding/trafficking defects we used confocal microscopy to see whether the subunits were able to reach the plasma membrane. Figure 4a shows the subcellular localization of wild type Kv2.1 and the double lysine mutation. While wild type Kv2.1 is clearly located at the periphery of the cell, the mutant subunits show intracellular staining indicating that this double lysine mutation generated folding/trafficking defects. Apparently, the interactions between T203K and S347K adversely affect the folding/trafficking of the Kv2.1 subunits.

A possible explanation for the observation that a pair of repulsive acidic residues was tolerated whereas repulsive

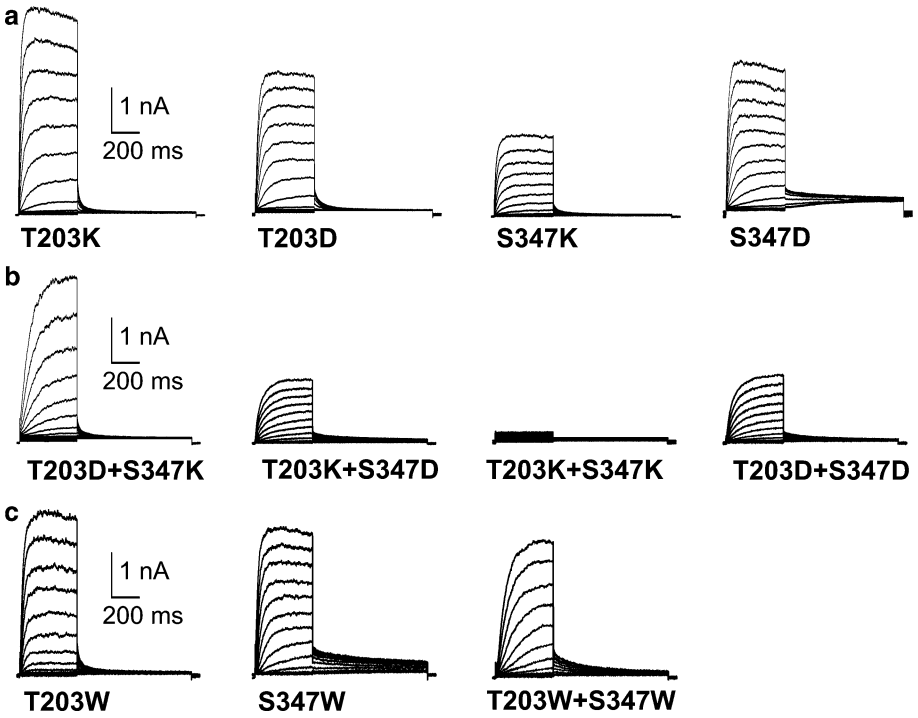


**Fig. 3** Whole-cell current recordings of **a** single charge, **b** double charge, and **c** tryptophan substitutions in Kv2.1. The holding potential was −80 mV, and cells were depolarized in 10 mV increments from −60 to +70 mV, 500 ms in duration, followed by a repolarizing pulse at −25 mV, 850 ms in duration. All mutations resulted in functional channels, with the exception of T203K + S347K

basic residues were not, is the much larger side chain volume of a lysine compared to an aspartate (Van der Waals volume of 108 and 51 $Å^3$ for lysine and aspartate side chains, respectively). To test whether the volume of the side chain itself was important, T203 and S347 were mutated to tryptophan, the amino acid with the bulkiest side chain (Van der Waals volume of 167 $Å^3$). The single mutations, T203W and S347W, were tolerated and resulted in functional channels with altered biophysical properties compared to WT Kv2.1 (Fig. 3c; Table 1). The double tryptophan mutant T203W + S347W also displayed outward currents (Fig. 3c) and double mutant cycle analysis gave a $\Delta\Delta G_0$ value of 0.8 ± 0.3 kcal/mol ($n = 12$). These results suggest that the volume of the residue side chain may play a role. However, since the volume of a tryptophan is much larger than that of a lysine the nonfunctionality of the double lysine mutant T203K + S347K can hardly be due to steric hindrance and most likely involves repulsive electrostatic effects.

The observation that a pair of repulsive acidic residues (T203D + S347D) was tolerated, whereas repulsive basic residues (T203K + S347K) were not, could also be due to the involvement of another charged residue in the neighborhood of these charges. A positive charge would enhance the repulsion between the double lysine mutations, resulting in nonfunctionality of the T203K + S347K mutation channel. In contrast, it would weaken the repulsion between the double aspartate mutation, resulting in the functional T203D + S347D mutation. We used the crystal structure of Kv1.2 to explore the charged residues of Kv2.1 that are located close to the S1 and S5 segments. In this structure, S1 and S5 are located close to the S4 segment. If a positive charge of the S4 segment enhanced the repulsion between the double lysine mutations, then changing this residue to a negatively charged glutamic acid should weaken the repulsion, resulting in a functional channel. To test our hypothesis, we made several charge reversal mutations in S4 (R293E + R294E, R300E, R303E, and R306E) in an attempt to rescue the nonfunctional T203K + S347K mutation. This approach has already been successfully used to demonstrate the charge network between negative charges in the S2 and S3 segments and positive S4 charges (Tiwari-Woodruff et al. 1997). The mutations R293E + R294E, R303E, and R306E were not able to restore the functionality of the T203K + S347K mutation (data not shown). In contrast, 4 out of 11 cells expressing R300E in the T203K + S347K background gave rise to a small outward $K^+$ current upon depolarization (Fig. 4b). For other voltage-gated $K^+$ channels, such as hERG, it has been described that expressing mutant channel subunits overnight at room temperature often results in enhanced expression of the channels (Anderson et al. 2006; Paulussen et al. 2002; Royal et al. 2005; Swiatecka-Urban et al. 2005; Zhou et al. 1999). Therefore,

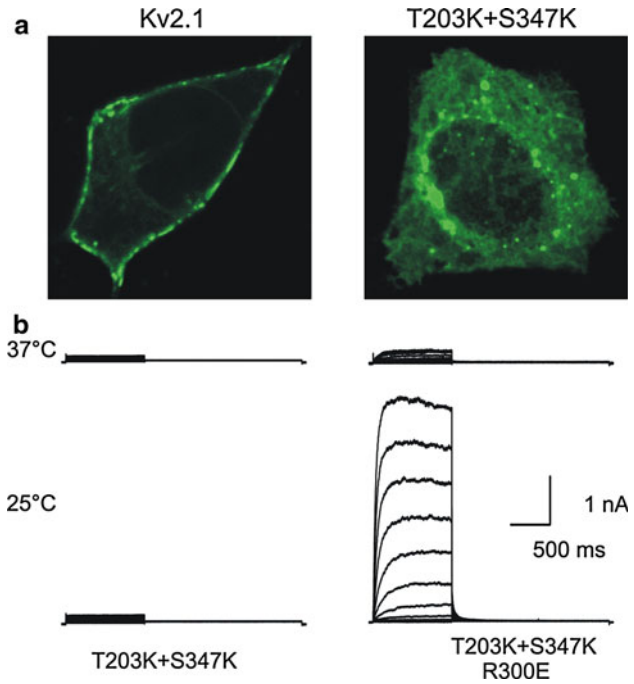


**Fig. 4a, b** Subcellular localization and whole-cell current recordings of T203K + S347K and the R300E rescue mutation. **a** Subcellular localization of WT Kv2.1 and T203K + S347K. Typical confocal images from cells expressing GFP-tagged Kv2.1 (*left*) and T203K + S347K (*right*) subunits. Kv2.1 channels were located at the periphery of the cell. The double lysine mutation was not functional and showed intracellular staining, suggesting a folding/trafficking defect. **b** Whole-cell current recordings of T203K + S347K and the R300E rescue mutation from cells grown overnight at 37°C and 25°C. The holding potential was −80 mV, and cells were depolarized in 10 mV increments from −60 to +70 mV, 500 ms in duration, followed by a repolarizing pulse at −25 mV, 850 ms in duration. The *scale bar* applies to all panels. When the cells were cultured in the standard conditions at 37°C, R300E in the T203K + S347K background gave rise to small outward $K^+$ currents upon depolarization. In contrast, culturing the cells overnight at 25°C resulted in large currents for the R300E mutation

we repeated the experiments with the T203K + S347K mutant and all the S4 mutations expressing them in an overnight culture at 25°C. Again, R293E + R294E, R303E, and R306E failed to restore the functionality in the T203K + S347K background. But for R300E in the T203K + S347K background, all cells tested under these conditions ($n = 19$) gave rise to outward $K^+$ currents (Fig. 4b). This observation favors the idea that the R300E mutation restores an underlying folding/trafficking deficiency. The triple mutant displayed altered biophysical properties compared to WT Kv2.1 channels (Table 1), but double mutant cycle analysis was precluded because the double lysine mutant T203K + S347K did not express (even after overnight culture at 25°C). The observation that the negative charge at position 300 in the S4 helix is able to weaken the interactions between T203K and S347K suggests close contact among T203 of S1, S347 of S5, and R300 of S4 in the Kv2.1 structure. To confirm the proximity of these residues we introduced the R300E mutation in the T203D + S347D background. If these residues are in close contact, the negative R300E mutation would make the double negative mutant nonfunctional. As expected, no current activation was observed after expressing this triple negative mutant (T203D + S347D + R300E) overnight at either 37 or 25°C (data not shown).

To visualize the position of the residues within the channel protein, a homology model for Kv2.1 was constructed independently from the above results using the crystal structure of the modified Kv1.2 (which contains the voltage-sensor paddle of Kv2.1) as template (see "Methods") (Long et al. 2007) (Fig. 5a). Kv2.1 residues V72-D80 (part of NAB domain), R150-A169 (part of linker between NAB domain and S1), and L211-N226 (S1–S2 linker) were omitted from the model, as no structural data were available for these nonconserved loops. We then investigated the location of T203 and S347 in this model. T203 of S1 and S347 of S5 are indeed located close to each other, at least in the open state of the channel (Fig. 5a, b). However, this proximity is not within the same subunit, but rather T203 from one subunit locates closely to S347 of its neighboring subunit. Both T203 and S347 do point towards the S4 segment, consistent with the interference of an S4 charge (R300).

## Discussion

Kv channel α-subunits can be generally divided into two groups: one with subunits that are able to form functional voltage-gated $K^+$ channels on their own (i.e., Kv2.1) and another group that do not and are therefore termed silent subunits (i.e., Kv6.4). A previous study that characterized the channel regions important for converting a functional Kv α-subunit into a silent one and vice versa indicated a remarkable functional tolerance in those Kv2.1 chimeras that included a single transmembrane segment from Kv6.4 (Ottschytsch et al. 2005). However, the combined exchange of the S1 and S5 segments was not tolerated (Fig. 1). To investigate which specific residues are responsible and most likely to interact with each other, we substituted the S1 or S5 residues that differed between Kv6.4 and Kv2.1 for Kv2.1 residues in the S1/S5 chimera. Individual back substitutions showed that the residue mutations A200V and A203T in the S1 segment and T343M and P347S in the S5 segment were important determinants.

To visualize the location of these residues, we generated a 3D Kv2.1 homology model (Fig. 5a) based on the Kv1.2-Kv2.1 paddle chimera structure (Long et al. 2007). The structure of Kv1.2 has been used as a model for various Kv

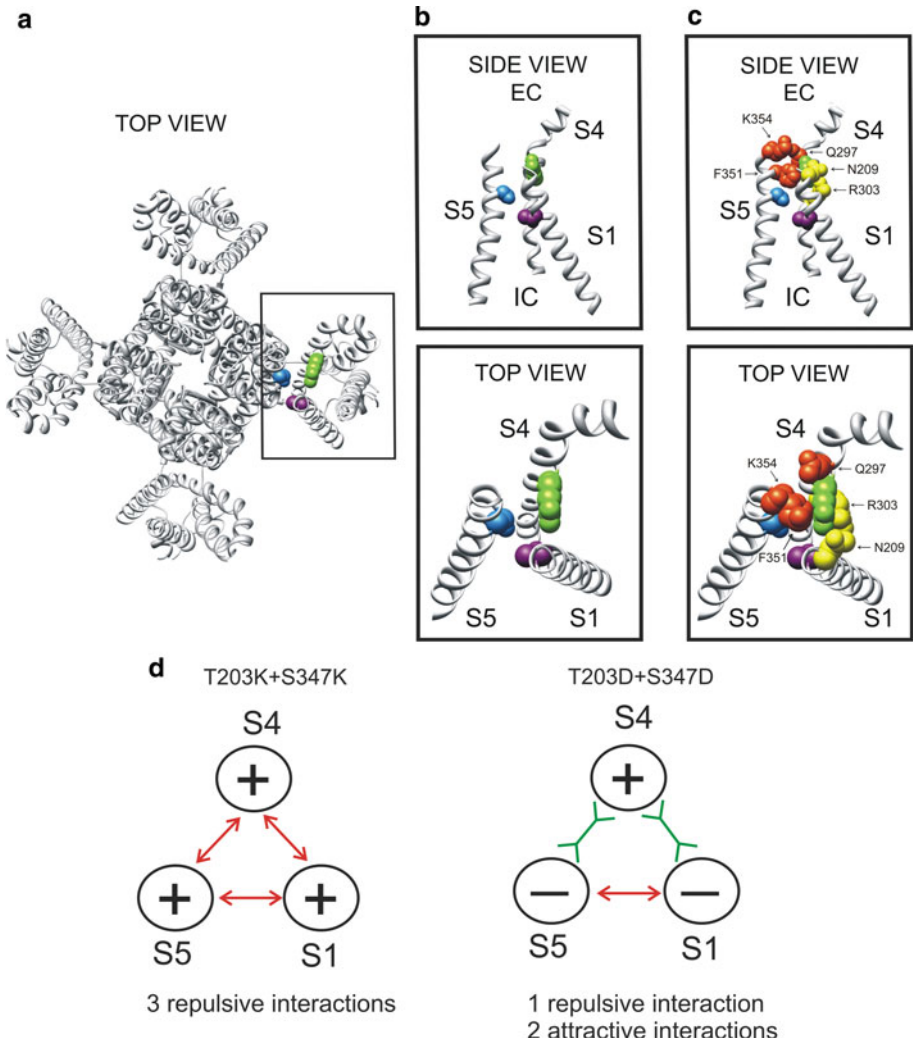


**Fig. 5a–d** Homology model of the human Kv2.1 channel in the open state. **a** Top view of the Kv2.1 tetramer. The residues T203 in S1, R300 in S4, and S347 in S5 are colored *purple*, *green*, and *blue*, respectively. Note that these residues are closely located in the Kv2.1 model, but this is not within the same subunit: T203 and R300 of one subunit are closely located to S347 of a neighboring subunit. **b** Enlarged top and side view of the S1–S4–S5 area that is *boxed* in **a**. **c** Same enlarged top and side view as in **b** in which the interacting S1–S4–S5 residues reported by Long et al. (2007) and Phillips and Swartz (2010) are shown as yellow and red residues, respectively. In **b** and **c** the same color code has been used as in **a** to designate the different residues. *EC* Extracellular, *IC* intracellular. **d** Hypothetical electrostatic interactions in the double lysine and double aspartate mutants. In the double lysine mutant (*left*), the positively charged S4 segment reinforces the repulsion between the lysines. The three repulsive interactions would cause a distortion of the channel, resulting in a loss of function. In the double aspartate mutant (*right*), there is only one repulsive interaction and the positive charge from S4 segment weakens this repulsion

channels. In this regard, caution should be taken, especially in case of channels in which the S1–S6 sequence does not show strong homology to Kv1.2 (e.g., KCNQ family ~20% identity, HERG ~10% identity). Kv2.1 shows a higher degree of homology to the Kv1.2 channel (~40% identity with Kv1.2). Furthermore, the fact that replacing the voltage-sensor paddle of Kv1.2 with the one from Kv2.1 leads to a functional channel indicates that the structures of both channels are sufficiently similar. Therefore, we considered that it was reasonable to use the structure of the modified Kv1.2 (already containing parts of Kv2.1) as a starting point for our Kv2.1 model. The model shows that residues T203 and S347 locate indeed in the vicinity of each other (Fig. 5a, b). The model is also in agreement with the results of the alanine scan that has been performed on the S1–S4 segments of Kv2.1 (Li-Smerin et al. 2000b), but the interaction between S1 (of one subunit) and S5 (of a neighboring subunit) appears to occur between adjacent subunits (Fig. 5a, b), a possibility that was not taken into account previously.

To determine lipid-protein and protein-protein interfaces in the S1 segment, two different scans have been

performed: a tryptophan scan (which causes sterical hindrance in protein-protein interfaces) in *Shaker* (Hong and Miller 2000) and an alanine scan (which can disrupt interactions between protein-protein interfaces) in Kv2.1 (Li-Smerin et al. 2000b). Both scans favored an α-helical configuration for S1 and indicated that one side of the helix faces the protein, while the other side faces the lipid bilayer. The residues of the S1/S5 chimera that were found to be critical for the functionality of the chimera (Fig. 2d) were indeed located on the sides of the transmembrane segments that have previously been proposed to face other regions of the channel protein (Hong and Miller 2000; Li-Smerin et al. 2000b). A similar tryptophan scan of S5 has been performed in *Shaker* to investigate which residues were facing lipid and which were facing the S1–S4 segment (Li-Smerin et al. 2000a). In this scan, S412W of *Shaker* (the homologue of S347W in Kv2.1) was regarded as a residue that was localized at an interaction surface. Mutation of this S327 residue affected the biophysical properties of the Kv2.1 channel (Fig. 3; Table 1) supporting that this residue is likely situated at a protein-protein interface.

To test the interaction between residue T203 and S347 in Kv2.1 further and to investigate whether incompatibility at these residue positions is a determinant for channel assembly, we replaced both residues with cysteines (data not shown), charged residues, and tryptophans. The cysteine substitutions and the attempted cross-linking experiments were inconclusive. Based on the location of the residues within the model (Fig. 5a, b), the residues seem to be quite buried within the channel protein and therefore most likely not accessible for cross-linking experiments.

As an alternative approach to test the possible interaction between both residues we opted for charge substitutions. The mutation of both residues to a positively charged lysine or a negatively charged aspartate was tolerated but resulted in channels with altered gating kinetics, especially at position S347. This indicates that both residues are indeed crucial positions for functionality, and mutation alters the channel gating kinetics either directly or through an allosteric effect. To test further for interactions, we substituted both residues simultaneously with a negatively charged aspartate or a positively charged lysine. We hypothesized that when both residues are in close contact, a similar charge would lead to repulsion and the effects on channel gating would be more pronounced. Indeed double mutant cycle analysis yielded a $\Delta\Delta G$ value of 1.36 kcal/mol (Table 1), which means that for the double negative charged mutant T203D + S347D, the combined effect was more pronounced than that of summing the individual effects. This indicates that both residues affect the same rate-limiting or consecutive transition step(s) (Mildvan et al. 1992). This energetic coupling strongly supports a functionally relevant interaction and possibly a close contact, but is not absolute proof of a direct interaction. Combining the positive charges was not tolerated and the double lysine mutant T203K + S347K resulted in a folding or trafficking deficiency (Fig. 4a). While this result precluded double mutant cycle analysis, it did support that these two specific S1 and S5 residue positions are important determinants for channel maturation. The two combinations of both a positive and a negative charge resulted in functional channels (Fig. 3b), and for T203K + S347D double mutant cycle analysis resulted in a $\Delta\Delta G$ value of 0.98 kcal/mol (Table 1), which was very close to the chosen cut-off value of 1 kcal/mol for coupling, further supporting a relevant interaction. To test further whether the difference between the double aspartate and lysine mutations was due to a steric effect or due to the increase in side chain volume, both residues were also replaced with a tryptophan. Both the individual mutations and the double tryptophan mutant were tolerated, indicating that the problem with the double lysine mutant could not be explained on this basis.

Kv channels contain two well recognizable regions, a pore-forming domain (S5–S6) and a voltage-sensing (S1–S4) domain that reorients as a result of changes in the membrane potential. These voltage sensor movements are translated into pore opening or closure through an electromechanical coupling. At present it remains unclear how the voltage-sensing S1–S4 segments are exactly positioned against the pore region. Mutagenesis studies have shown that the intracellular interface between the S4–S5 linker and S6 is important for coupling voltage sensor movements with pore gating (Labro et al. 2008; Lu et al. 2002). However, to transfer the VSD movement over the S4–S5 linker onto the S6 segment adequately, the rest of the VSD cannot be moving freely with respect to the pore domain and needs to have at least one other anchoring point. By using the paddle chimera, which consists of the Kv2.1 voltage-sensor paddles (i.e., the S3b and S4 helices) in a Kv1.2 background, it has been demonstrated that interactions between S1 and the pore domain were also involved in channel gating (Lee et al. 2009; Long et al. 2007). In this paddle-chimera, the extracellular side of S1 makes specific contacts with the pore helix and the S5 helix. Based on the crystal structure of the paddle chimera, Long and colleagues showed that E189 of S1 interacts with R296 of S4 (N209 and R303 in hKv2.1, respectively; yellow residues in Fig. 5c) while Phillips and colleagues demonstrated in *Shaker* a close proximity between the residues A419 and F416 in S5 and R362 in S4 (F351, K354, and Q297 in hKv2.1, respectively; red residues in Fig. 5c) (Long et al. 2007; Phillips and Swartz 2010). The results presented in this study demonstrated a close contact between the more intracellularly located residues of S1 (T203) and S5 (S347)

than the contacts reported previously (Fig. 5c). Our data therefore indicate that the contact interface between S1 and the pore in Kv2.1 is more extensive than previously described and this may apply to other *Shaker*-type channels.

It is conceivable that distorting this anchoring point alters the conformation of the VSD and thus affects the gating kinetics. Therefore, the observed changes in channel gating by mutating residues T203 and S347 may be of an allosteric nature. Furthermore, mutations that strongly distort this anchoring most likely result in misfolded channel proteins, which we propose to be the case for T203K + S347K. However, although an allosteric effect may explain the observed effects on channel gating, a direct effect of the mutations on the movement of the S4 segment cannot be completely excluded. The results of a tryptophan scan of S5 in *Shaker* identified an extracellularly located cluster of residues that faces the S1–S4 voltage sensor domain (Li-Smerin et al. 2000a) and upon mutation slows down the activation of the voltage sensor suggesting a local interaction with S4 (Soler-Llavina et al. 2006). The location of our S347 residue in this corresponding region further favors the possibility of a direct effect on S4 movement.

To investigate whether the introduced charges affected the S4 voltage sensor, we combined the S1 and S5 charge mutation with S4 charge mutations. This showed that the trafficking/folding problem of the nonexpressing double lysine mutant T203K + S347K could be rescued by reversing the second R2 charge of the S4 segment (R300E) (Fig. 4b). The observation that lowering the incubation temperature from 37°C to 25°C resulted in a substantial increase in current for the triple mutant T203K + S347K + R300E further supports the idea that absence of current for T203K + S347K was due to a folding deficiency as the electrophysiological recordings were done at room temperature in both conditions (Fig. 4b). Conversely, combining this S4 R300E mutant with the double aspartate mutant T203D + S347D, thus yielding three negative charges, resulted likewise in a channel mutant that did not translocate properly from the ER to the plasma membrane (even after lower incubation temperature). These results indicate that at a certain moment in the channel biogenesis the three charges of S1, S5, and the S4 voltage sensor affect each other.

Why did mutating A203 or P347 in the nonfunctional S1/S5 chimera back to the corresponding Kv2.1 residues (T203 and S347, respectively) rescue channel functionality? One possibility may be because of the partial electronegativity of the OH side chain of both S and T residues. Furthermore, also tryptophan residues (with their pi-electron cloud) and cysteine residues are partially polar explaining why both double mutants T203W + S347W and T203C + S347C were tolerated. Although speculative, all the data fit with an interaction scheme that involves electrostatic interactions among residues T203 (in S1), S347 (in S5), and R300 (in S4) (Fig. 5d). In the nonfunctional S1/S5 chimera, it was sufficient to revert one of nonpolar residues A203 or P347 back to their Kv2.1 counterparts to rescue the function. In the above interaction scheme, this implies that having partial electronegativity either at position 203 or 347 is sufficient to restore channel maturation.

In conclusion, our results indicate that the residues T203 in the S1 segment and R300 in the S4 segment of one subunit and residue S347 in the S5 segment of a neighboring subunit are located close to each other in the Kv2.1 channel. Furthermore, by mutating T203 and S347 to charged residues we showed that a network of electrostatic interactions can be generated among T203 (S1), R300 (S4), and S347 (S5). Finally, our data indicate that the S1-pore contact interface in the Kv2.1 channel is more extensive than previously described, and this may apply to other Shaker-type channels.

**Acknowledgments** We would like to thank Tessa de Block, Carole Faghel, Evy Mayeur, and Tine Bruyns for their excellent technical assistance, and Adam Raes for helpful discussions in the early phase of this study. This work was supported by the 'Fonds voor Wetenschappelijk Onderzoek Vlaanderen' Grants FWO-G.0152.06, FWO-1.5.055.08, and FWO-G.0449.11; the IAP6/31 grant of the Interuniversity Attraction Poles Program–Belgian State–Belgian Science Policy; a concerted research project Grant BOF-GOA 2004 of the University of Antwerp; and a BOF-TOP08 project of the University of Antwerp.

## References

Anderson CL, Delisle BP, Anson BD, Kilby JA, Will ML, Tester DJ, Gong Q, Zhou Z, Ackerman MJ, January CT (2006) Most LQT2 mutations reduce Kv11.1 (hERG) current by a class 2 (trafficking-deficient) mechanism. Circulation 113:365–373

Bezanilla F (2000) The voltage sensor in voltage-dependent ion channels. Physiol Rev 80:555–592

Doyle DA, Cabral JM, Pfuetzner RA, Kuo A, Gulbis JM, Cohen SL, Chait BT, MacKinnon R (1998) The structure of the potassium channel: molecular basis of $K^+$ conduction and selectivity. Science 280:69–77

Durell SR, Shrivastava IH, Guy HR (2004) Models of the structure and voltage-gating mechanism of the *shaker* $K^+$ channel. Biophys J 87:2116–2130

Gandhi CS, Isacoff EY (2002) Molecular models of voltage sensing. J Gen Physiol 120:455–463

Guex N, Peitsch MC (1997) SWISS-MODEL and the Swiss-PdbViewer: an environment for comparative protein modeling. Electrophoresis 18:2714–2723

Gutman GA, Chandy KG, Grissmer S, Lazdunski M, McKinnon D, Pardo LA, Robertson GA, Rudy B, Sanguinetti MC, Stuhmer W, Wang X (2005) International Union of Pharmacology LIII. Nomenclature and molecular relationships of voltage-gated potassium channels. Pharmacol Rev 57:473–508

Hamill OP, Marty A, Neher E, Sakmann B, Sigworth FJ (1981) Improved patch clamp techniques for high-resolution current recording from cells and cell-free membrane patches. Pflugers Arch Eur J Physiol 391:85–100

Heginbotham L, Lu Z, Abramson T, MacKinnon R (1994) Mutations in the $K^+$ channel signature sequence. Biophys J 66:1061–1067

Hong KH, Miller C (2000) The lipid-protein interface of a Shaker K(+) channel. J Gen Physiol 115:51–58

Jiang Y, Lee A, Chen J, Ruta V, Cadene M, Chait BT, MacKinnon R (2003) X-ray structure of a voltage-dependent $K^+$ channel. Nature 423:33–41

Labro AJ, Raes AL, Grottesi A, Van HD, Sansom MS, Snyders DJ (2008) Kv channel gating requires a compatible S4–S5 linker and bottom part of S6, constrained by non-interacting residues. J Gen Physiol 132:667–680

Lee SY, Banerjee A, MacKinnon R (2009) Two separate interfaces between the voltage sensor and pore are required for the function of voltage-eependent K(+) channels. PLoS Biol 7:e47

Li-Smerin Y, Hackos DH, Swartz KJ (2000a) A localized interaction surface for voltage-sensing domains on the pore domain of a $K^+$ channel. Neuron 25:411–423

Li-Smerin Y, Hackos DH, Swartz KJ (2000b) Alpha-helical structural elements within the voltage-sensing domains of a K(+) channel. J Gen Physiol 115:33–50

Long SB, Campbell EB, MacKinnon R (2005) Crystal structure of a mammalian voltage-dependent *Shaker* family $K^+$ channel. Science 309:897–903

Long SB, Tao X, Campbell EB, MacKinnon R (2007) Atomic structure of a voltage-dependent K+ channel in a lipid membrane-like environment. Nature 450:376–382

Lu Z, Klem AM, Ramu Y (2002) Coupling between voltage sensors and activation gate in voltage-gated $K^+$ channels. J Gen Physiol 120:663–676

Mildvan AS, Weber DJ, Kuliopulos A (1992) Quantitative interpretations of double mutations of enzymes. Arch Biochem Biophys 294:327–340

Ottschytsch N, Raes A, Van Hoorick D, Snyders DJ (2002) Obligatory heterotetramerization of three previously uncharacterized Kv channel alpha-subunits identified in the human genome. Proc Natl Acad Sci USA 99:7986–7991

Ottschytsch N, Raes AL, Timmermans JP, Snyders DJ (2005) Domain analysis of Kv6.3, an electrically silent channel. J Physiol 568:737–747

Paulussen A, Raes A, Matthijs G, Snyders DJ, Cohen N, Aerssens J (2002) A novel mutation (T65P) in the PAS domain of the human potassium channel HERG results in the long QT syndrome by trafficking deficiency. J Biol Chem 277:48610–48616

Phillips LR, Swartz KJ (2010) Position and motions of the S4 helix during opening of the Shaker potassium channel. J Gen Physiol 136:629–644

Royal DC, Bianchi L, Royal MA, Lizzio M Jr, Mukherjee G, Nunez YO, Driscoll M (2005) Temperature-sensitive mutant of the *Caenorhabditis elegans* neurotoxic MEC-4(d) DEG/ENaC channel identifies a site required for trafficking or surface maintenance. J Biol Chem 280:41976–41986

Soler-Llavina GJ, Chang TH, Swartz KJ (2006) Functional interactions at the interface between voltage-sensing and pore domains in the Shaker K(v) channel. Neuron 52:623–634

Swiatecka-Urban A, Brown A, Moreau-Marquis S, Renuka J, Coutermarsh B, Barnaby R, Karlson KH, Flotte TR, Fukuda M, Langford GM, Stanton BA (2005) The short apical membrane half-life of rescued ΔF508-cystic fibrosis transmembrane conductance regulator (CFTR) results from accelerated endocytosis of ΔF508-CFTR in polarized human airway epithelial cells. J Biol Chem 280:36762–36772

Tiwari-Woodruff SK, Schulteis CT, Mock AF, Papazian DM (1997) Electrostatic interactions between transmembrane segments mediate folding of *Shaker* $K^+$ channel subunits. Biophys J 72:1489–1500

Vriend G (1990) WHAT IF: a molecular modeling and drug design program. J Mol Graph 8:52–56

Yifrach O, MacKinnon R (2002) Energetics of pore opening in a voltage-gated k(+) channel. Cell 111:231–239

Zhou Z, Gong Q, January CT (1999) Correction of defective protein trafficking of a mutant HERG potassium channel in human long QT syndrome. Pharmacological and temperature effects. J Biol Chem 274:31123–31126